Acta Technica *62* (2017), No. 7A, 323–334

Dynamic data modeling and simulation method of machine system based on grid finite element analysis

Huachuan Li[1], Zhugao Pang[2], Huijie Yu[3]

Abstract. The impact mechanical system of a new hydraulic power piling machine is researched and a dynamic data modeling and simulation method of mechanical system based on meshing finite element analysis is proposed. Based on a large number of research literatures on impact mechanical system dynamics at home and abroad, the finite volume method discrete equation is used and the Galerkin discrete finite element is adopted to approach it by mechanical elasticity equation to obtain the 3D unstructured mesh model of impact mechanical system of hydraulic power piling machine. The impact piling force of impact mechanical system of hydraulic power piling machine and meshing finite element of key parts are researched, including the punch hammer, tension and compression box, pull rod, pile caps etc. Finally, the LS-DYNA dynamics simulation software is used to simulate the finite elements for the impact mechanical system of hydraulic power piling machine. The results show the proposed method is effective.

Key words. Meshing, Finite elements, Mechanical system, Modeling and simulation.

1. Introduction

Among the environmental test devices, the vibration, impact, acceleration and swing test devices are dynamic test devices. The system characteristics of dynamic test devices are relatively complicated and multiple parameters are mutually combined, mainly including the frequency functions, which makes the design difficult. Only the simplified design calculation based on the analytic formula is used for the earlier design technique. Taking the servo valve of hydraulic vibration platform as an example, the load impact is not taken into consideration in the output flow calcu-

[1]Department of mechanical engineering , Guangxi technological college of machinery and electricity, GUANGxi nanning, 530007, China

[2]School of mechanical engineering, Guangxi University, GUANGxi nanning, 530004, China

[3]School of mechanical engineering , University of shanghai for science and technology, shanghai, 200093, China

lation or the load is processed based on a fixed value. But in fact, the load is changed all the time. For the servo valve, with increasing of frequency, the flow will decrease and the phase lag will continuously increase. The phase lag has a significant impact on the system stability. Such simplified design method cannot carefully and completely predict and understand the dynamic characteristics of system. Therefore, the system design risks can be increased.

The simulation technique is an effective means to analyze the dynamic system. Such simulation technique incorporates various related dynamic variables into a differential equation, uses model (circuit or software) to express the dynamic characteristics of system and operates the model to obtain variable-time changing curve. Latterly, with the development of all-digital simulation technique, the differential equation and each nonlinear link or module can enter into the system model. Therefore, the degree of simulation is further increased. With popularization of microcomputer and simulation software, the simulation technique is increasingly used in all walks of life. Several examples are used in this paper to introduce the application of simulation technique in design of dynamic environment test device. The simulation technique has experiences the analog computer, hybrid digital-analog computer and all-digital computer. In 1946, the analog computer was invented in America, which could simulate different physical phenomenon, such as the flight path of missile and airplane etc. It indicates the beginning of analog simulation technique. Since then, many analog machines came forth. The period from the 1950s to 1560s is the golden age for analog computer. Although the analog computer obtains a great success, many problems are exposed, such as insufficient data accuracy, difficulty in realizing the interpolation function and failure of satisfaction of data control system requirements etc. In the end of the 1950s, the hybrid analog computer appeared due to the development requirements of missile technology. The period from the 1960s to middle 1970s is the flourishing age of hybrid analog computer. America ADI Company invented the all-digital simulation computer AD10 in 1978, which indicates that the all-digital simulation computer takes the lead in fierce competition of hybrid analog computer and digital analog computer and the new era of all-digital simulation comes. In 1973, the special hydraulic simulation software HYDSIM was successfully invented in America. Then, the hydraulic simulation software was continuously developed and improved in Europe and America. In 1980, DSH (Germany) and HASP (the UK) etc. were successively issued. On October 15, 1985, the first all-digital simulation computer "Yinhe I Simulation Computer (YH-F1)" was successfully invented in China, which indicates China enters an all-digital simulation era. Hereafter, many new simulation computers appears. The simulation technique is firstly used in aerospace field which is the birthplace of simulation computer. Only the important and complex dynamic system design can be affordable. After popularization of microcomputer and graphical programming of simulation software, the simulation technique is widely used and the symbolic node is issuance of MATLAB/Simulink simulation software. MATLAB/Sim-Mink plays an important part in simulation software. It can be considered that Simulink is the watershed. Before such period, the modeling is based on statement description, the relationship between modules is defined based on the statement and the sys-

tem module composition and relationship between modules cannot be visually seen. Simulink provides a graphic modeling method and the complex simulation model can be built only by simple mouse drag operation. Its appearance is presented by block chart and the layered structure is used. In the view of modeling, it is applicable to top-down design process (from concept, function, system, subsystem to device) bottom-up reverse process design. In the view of analysis research, the Simulink not only enables the users know the dynamic details of specific links, but also clearly understands the information exchange between each device, subsystem and system and grasps interaction between each part. It is very convenient for modeling and beneficial to error-checking and correction of model. Except quick and convenient modeling, other functions are powerful as well. For example,, it can process different systems, including the linear and nonlinear system; discrete, continuous and hybrid system; single-task and multi-task discrete event system. Simulink 6.5 is the milestone version and its acceleration mode can make the computing speed increase several tens of times and hundred times.

The finite element and boundary element method is often used in mechanical dynamics analysis and the finite volume method combined with hydromechanics modeling method is also adopted, such as the finite element and extended finite element etc. It is very difficult to implement stable discretization for the nonlinear problems. The parameter stabilization is carried out in literature [10] to obtain the stabilization equation for contact mechanical problems. The Nitsche processing method is proposed in literature [11] and such method can be considered as consistent penalty function method. When the model parameters are suitably selected, the corresponding discrete equation set can be well adjusted. The impact mechanical system of a new hydraulic power piling machine is researched and a dynamic data modeling and simulation method of mechanical system based on meshing finite element analysis is proposed in this paper. The LS-DYNA dynamics simulation software is used to simulate the finite elements for the impact mechanical system of hydraulic power piling machine. The results show the proposed method is effective.

2. Vibration dynamic model of mechanical system of piling machine

In wave mechanics model, the pull rod and precast pile used in the impact mechanical system of hydraulic power piling machine is simplified as the elastic rod, where the transmission reflection of stress wave in pull rod is taken into consideration when the pull rod is simplified as the elastic rod, which makes the complex wave mechanics model and complicated solution procedure. The vibration mechanics theory is used to simplify the pull rod as single spring-single mass block system and then the vibration mechanics model more simple and convenient than wave mechanics model can be built to obtain impact pilling force. As the complexity of mechanical model will not be increased if the precast pile is simplified as elastic rod, the precast pile is still assumed as elastic rod with equal wave drag in wave mechanics model.

According to the vibration mechanicals theory, the pull rod is simplified as the system composed of single mass unit and single spring unit (rigidity of pull rod),

namely, the pull rod is simplified as a system with single degree of freedom. The pull rod mass unit is set as m4 (the mass is uniformly distributed on pile cap, tension and compression box) and the equivalent rigidity is set as k2. Other assumptions are same as wave mechanics model assumption. The structure of impact mechanical system of hydraulic power piling machine can be simplified as shown in Fig. 1.

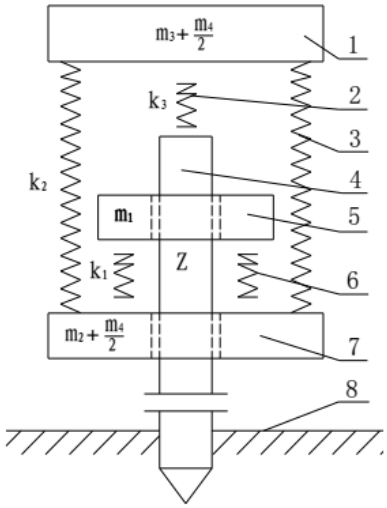

Fig. 1. Structure model of impact mechanical system of piling machine
(1. Pile cap; 2. crash pad; 3. pull rod (spring); 5. punch hammer; 6. buffer spring; 7. tension and compression box; 8. working medium)

3. Mechanical system dynamics modeling based on finite element

3.1. Mesh structure discretization solutions

The geometrical elements are used to conduct mesh generation. In general, the tetrahedron is used to represent the substrate and the triangle element is used to represent the stress surface. The two-dimensional model mesh is used in order to simplify description as shown in Fig. 2. But in fact, the design method is three dimensional.

In Fig. 2a, Ω refers to the physical region, Γ refers to the outer shape of model and Γ_f is defined as stress surface. In Fig. 2b, the triangle is used to represent the substrate and the heavy line represents mechanical contact area. This geometry mesh is applicable to mechanical problems. In Fig. 2c, the control volume is associated with each element in mesh. Pressure$p$, density ρ_f and viscosity μ_f are all associated with cell center. The displacement is unknown and u is associated with top point of substrate. In Fig. 2d, different nodes are used to represent the displacement on each side in mechanical contact area. In addition, the traction vector t is associated with each mechanical contact area surface.

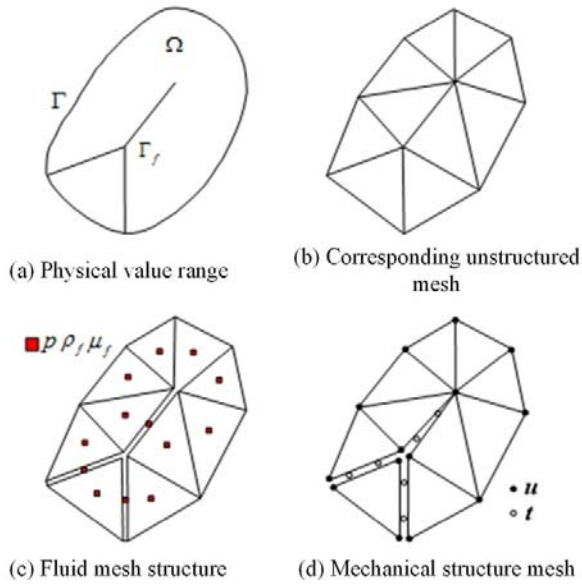

Fig. 2. Two-dimensional model mesh

3.2. Mechanics equation and model approximation in discrete mechanical contact area

The stress equation of finite volume method is used to conduct discretization. Based on the approximate magnetic flow on two points, the flow rate between two adjacent controlled quantities can represent the pressure differential function:

$$Q_{ij} = \lambda T_{ij}(p_i - p_j)\,. \tag{1}$$

Where, Q_{ij} is the mass flow rate between controlled quantity i and j. The dynamics fluidity can be defined as $\lambda = \rho_f/\mu_f$. The geometric transfer part is T_{ij}. The approximation scheme of finite volume of backward Euler time and flow rate is adopted and the flow rate equation (1) can be approximated as:

$$\frac{p_f i^{n+l}\phi_i^{n+1} - p_{fi}^n \varphi_i^n}{\Delta t} V_i = \sum_j Q_{ij} + q_i v_i\,. \tag{2}$$

Where, V_i is volume i and the time interval is Δt. The index $n+1$ and n respectively refer to the current and next step.

3.3. Quasi-static mechanical elasticity equation

Under the case of external boundary Γ and internal boundary Γ_f, the potential energy of mechanical contact defined in formula (2-3) can be further represented as:

$$\begin{aligned}\Pi =&\frac{1}{2}\int_{\Omega}\boldsymbol{\varepsilon}:\boldsymbol{\sigma}d\Omega-\int_{\Omega}\boldsymbol{u}\rho\boldsymbol{g}d\Omega-\int_{\Gamma}\boldsymbol{u}\bar{t}d\Gamma\\&-\int_{\Gamma_f}\boldsymbol{u}^{+}\bar{\boldsymbol{t}}_f^{+}d\Gamma-\int_{\Gamma_f}\boldsymbol{u}^{-}\bar{\boldsymbol{t}}_f^{-}d\Gamma\,.\end{aligned}\tag{3}$$

Where, $\bar{\boldsymbol{t}}$ is the total traction vector on boundary Γ. The total traction force $\bar{\boldsymbol{t}}_f^{-}$ and $\bar{\boldsymbol{t}}_f^{+}$ are respectively in opposite side of fracture interface. Based on the continuity condition $\bar{\boldsymbol{t}}_f=\bar{\boldsymbol{t}}_f^{+}=\bar{\boldsymbol{t}}_f^{-}$, it can be obtained that:

$$\begin{aligned}\Pi =&\frac{1}{2}\int_{\Omega}\boldsymbol{\varepsilon}:\boldsymbol{\sigma}d\Omega-\int_{\Omega}\boldsymbol{u}\rho\boldsymbol{g}d\Omega-\int_{\Gamma}\boldsymbol{u}\bar{t}d\Gamma\\&-\int_{\Gamma_f}(\boldsymbol{u}^{+}-\boldsymbol{u}^{-})\bar{\boldsymbol{t}}_f d\Gamma\end{aligned}\tag{4}$$

Where, $\bar{\boldsymbol{t}}_f$ combines with the impact of mechanical pressure p and effective stress of Terzaghi $\boldsymbol{\sigma}'$.

$$\bar{\boldsymbol{t}}_f=-\boldsymbol{\sigma}\boldsymbol{n}=-(\boldsymbol{\sigma}-\boldsymbol{I}p)\boldsymbol{n}=t_N\boldsymbol{n}+t_T\boldsymbol{\tau}+p\boldsymbol{n}\,.\tag{5}$$

The gap function g can be expressed as the displacement function:

$$g=\boldsymbol{u}^{+}-\boldsymbol{u}^{-}=(g_N,g_T)\,.\tag{6}$$

Therefore, the following potential-energy function can be obtained:

$$\begin{aligned}\Pi =&\frac{1}{2}\int_{\Omega}\boldsymbol{\varepsilon}:\boldsymbol{\sigma}d\Omega-\int_{\Omega}\boldsymbol{u}\rho\boldsymbol{g}d\Omega-\int_{\Gamma}\boldsymbol{u}\bar{\boldsymbol{t}}d\Gamma\\&-\int_{\Gamma_f}g_N p d\Gamma-(\int_{\Gamma_f}g_N t_N+g_T t_T)d\Gamma\end{aligned}\tag{7}$$

The differential is used to calculate and obtain the minimum potential energy:

$$\begin{aligned}\delta\Pi =&\frac{1}{2}\int_{\Omega}\delta\boldsymbol{\varepsilon}:\boldsymbol{\sigma}d\Omega-\int_{\Omega}\delta\boldsymbol{u}\rho\boldsymbol{g}d\Omega-\int_{\Gamma}\delta\boldsymbol{u}\bar{\boldsymbol{t}}d\Gamma\\&-\int_{\Gamma_f}\delta g_N p d\Gamma-(\int_{\Gamma_f}g_N t_N+\delta g_T t_T)d\Gamma=0\,.\end{aligned}\tag{8}$$

The finite element approximation can be made based on the node. Therefore, the displacement can be defined as:

$$\boldsymbol{u}(\xi)\approx\sum_{a}N_a(\xi)\boldsymbol{u}_a\,.\tag{9}$$

Where, $\boldsymbol{u}_a$ is the node displacement value and N_a is the shape function. The

gap function of impact mechanical system of hydraulic power piling machine can be defined as:

$$\begin{aligned} g(\xi) &= \boldsymbol{u}^{+}(\xi) - \boldsymbol{u}^{-}(\xi) \\ &\approx \sum_{a} N_a(\xi)(\boldsymbol{u}_a^{+} - \boldsymbol{u}_a^{-}) = \sum_{a} N_a g_a \,. \end{aligned} \tag{10}$$

Where, $\boldsymbol{u}^{+}$ and $\boldsymbol{u}^{-}$ respectively refer to the displacement on both sides of mechanical contact area. The surface discretization can be expressed as $\Gamma_f = \cup_e \Gamma_{f,e}$ and the stress area can be expressed as:

$$\begin{aligned} &\int_{\Gamma_f} \delta g_N p d\Gamma - \int_{\Gamma_f} (\delta g_N t_N + \delta g_T t_T) d\Gamma \\ &\approx \sum_{e} \times \int_{\Gamma_{f,e}} \sum_{a} \delta(g_N)_a N_a p d\Gamma \\ &- \sum_{e} \times \int_{\Gamma_{f,e}} (\sum_{a} \delta(g_N)_a N_a t_N + \sum_{a} \delta(g_T)_a N_a t_T) d\Gamma \,. \end{aligned} \tag{11}$$

The traction vector (t_N, t_T) is shown above. Under the ideal condition, the friction law can be obtained based on Kuhn-Tucker relation:

$$\begin{cases} t_N \geq 0, g_N \geq 0, t_N g_N = 0, \dot{g}_T(\xi) - \eta \dfrac{\partial \Phi}{\partial t_T} = 0 \,, \\ \Phi = |t_T| - \mathcal{F}(t_N) \leq 0, \eta \geq 0, \Phi \leq 0, \eta \Phi = 0 \,. \end{cases} \tag{12}$$

It can be known that the slip phenomenon will occur when $\Phi = 0$; the adherence phenomenon will occur when $\Phi < 0$ and $\dot{g}_T = 0$. The Kuhn-Tucker constraint and adherence/slip rules can be replaced with:

$$\begin{cases} \dot{g}_T(\xi) - \eta \dfrac{\partial}{\partial t_T} \Phi = \dfrac{1}{\varepsilon_T} \dot{t}_T \\ t_N = \varepsilon_N g_N, \eta \geq 0, \Phi \leq 0, \eta \Phi = 0 \,. \end{cases} \tag{13}$$

Where, $\varepsilon_N \gg 1$, $\varepsilon_T \gg 1$ is penalty factor. ε_N is influence by man-made rigidity on stress surface. Based on the above formula, it can be known that the stress will occur when $g_N > 0$.

In deformation process, the contact area is directly proportional to the force imposed. Therefore, for the normal contact surface, the following formula is satisfied:

$$\mathcal{N}(g_N) = \frac{k_n g_0}{g_0 \cdot g_N} g_N \,. \tag{14}$$

Where, k_n is the initial normal rigidity. Under the "ideal" condition, the surface

roughness contact can be considered as below:

$$\begin{cases} t_N = \mathcal{N}(g_N), g_N \leq g_0\,, \\ \dot{g}_T - \eta \dfrac{\partial}{\partial t_T}\Phi = \dfrac{1}{\varepsilon_T} i_T \\ \eta \geq 0, \Phi \leq 0, \eta\Phi = 0\,. \end{cases} \tag{15}$$

The return mapping algorithm can be used to assess the traction vector as below:

$$\begin{cases} t_N^{n+1} = N(g_N^{n+1})\,, \\ t_T^{trial} = t_T^n + \varepsilon_T(g_T^{n+1} - g_T^n)\,, \\ \Phi^{trial} = |t_T^{trial}| - \mathcal{F}(t_N^{n+1})\,, \\ t_T^{n+1} = t_T^{trial}, if\Phi^{trial} \leq 0\,, \\ |t_T^{n+1}| = \mathcal{F}(t_N^{n+1}), if\Phi^{trial} > 0\,. \end{cases} \tag{16}$$

Where, the subscript $n+1$ and n respectively refers to the current and previous step.

4. Experimental analysis

4.1. Mesh model building

The hypermesh with powerful mesh generation function is selected to conduct mesh generation for the three-dimensional model of impact mechanical system. The good model will be built for the impact mechanical system of hydraulic power piling machine in Pro/E, the model is imported into Hypermesh, the surface mesh is firstly built for each part in Hypermesh, the high-precision hexahedral mesh can be obtained after tension and adjustment of surface mesh, where 3D solid element solid164 is used for the mesh element, the key part material and its overall model mesh are shown in Fig. 3a-d. Fig. 3a is the punch hammer mesh model, Fig. 3b is the tension and compression box mesh model, Fig. 3c is the local mesh model of pile cap and pull rod and Fig. 3d is the local mesh model of impact mechanical system. For the impact mechanical system model, the number of element is 89800 and the number of node is 124596.

Table 1. Material property of key parts

Name	Element type	Material	Elasticity modulus (Gpa)	Poisson ratio	Density (kg.mm/3)
Impact block	solid164	Steel	207GPa	0.28	7.83×10-6
Tension and compression box	solid164	Steel	207GPa	0.28	7.83×10-6
Pull rod	solid164	Steel	207GPa	0.28	7.83×10-6
Pile cap	solid164	Steel	207GPa	0.28	7.83×10-6
Precast pile	solid164	Concrete	30GPa	0.2	2.4×10-6

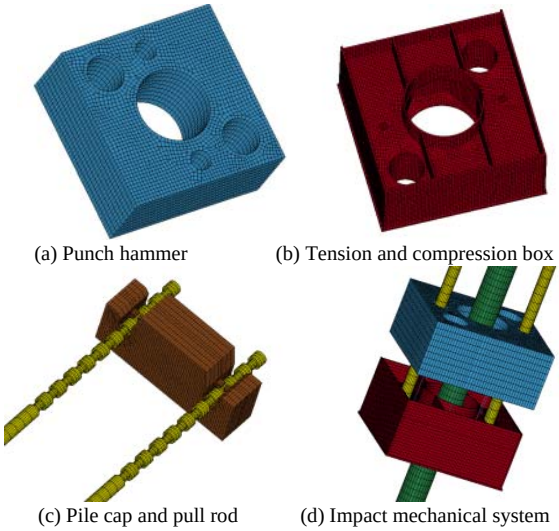

Fig. 3. Mesh model of key parts

The finite element mesh model of impact mechanical system of hydraulic power piling machine is imported into ANSYS to conduct pretreatment. The pretreatment process mainly includes the following septs:

(1) Establish part group: establish 7 part groups, namely, punch hammer, tension and compression box, pull rod, pile cap, pile, spring 1 and spring 2. Spring 1 is the spring rigidity between punch hammer and tension and compression box, namely, $k1 = 1{\times}109\text{N/m}$; spring 2 is the spring rigidity between pile cap and pile, namely, $k2 = 4{\times}108\text{N/m}$.

(2) Define the load and boundary conditions: add 6.12m/s of initial speed based on the design parameters of impact mechanical system of hydraulic power piling machine. Take no account of the impacts of soil layer on piling process in simulation; adopt full constraints in the bottom of precast pile.

(3) Establish the analysis options: set the computation time as 80ms, the output type as LS-DYNA and the output time interval as 0.2ms.

(4) Export setting: output the established simulation model in the format of K document; revise the contact and collision parameters etc. in the notebook and import the revised K document into LS-DYNASolver. As the impact process is transferred through spring, the automatic single face node-surface contact is adopted and the keyword is *CONTACT_AUTOMATIC_NODES_TO_SURFACE.

4.2. Impact piling force analysis

The contact surface element stress can be obtained from the finite element simulation results to calculate the piling force and compare with the theoretical value obtained above. Fig. 4a respectively represents the position of pile cap plane unit 45099 and the stress curve of such unit in axial direction (X direction) of precast pile. Fig. 4b represents the impact pile force curve under the theory of wave mechanics

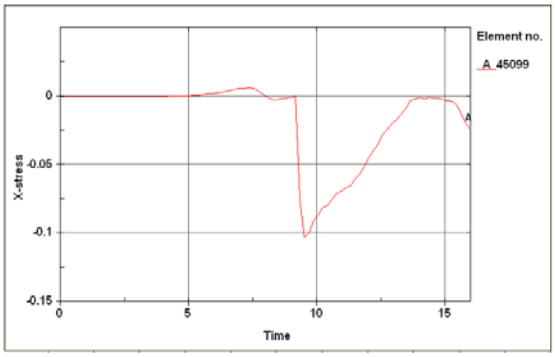

(a) The X direction stress curve of the unit 45099

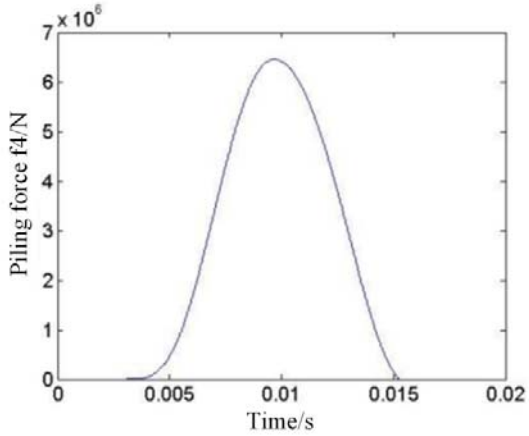

(b) The impact pile force curve under the theory of wave mechanics

Fig. 4. Impact pile force analysis

It can be known from Fig. 4a X-direction stress of unit 45099 is maximum at 9.5ms around. At this time, namely, in the simulation process, it is the occurrence time of maximum impact piling force. In Fig. 4b, the maximum impact piling force obtained under the theory appears in 0.01s, namely, 10ms around. By comparison with Fig. 4a and Fig. 4b, it can be known that the occurrence time of maximum impact piling force is basically consistent with the time of obtaining maximum impact piling force under the theory. However, in the theoretical results, the maximum impact piling force is 0.69×107N approximately, which is deviated from the result obtained through simulation. However, their occurrence time and variation tendency are basically similar. The structural features of each component have been taken into consideration in the simulation process. But the structural features are ignored in theoretical model. For example, the groove on top of pull rod, the clamping device between pile cap and pull rod and each rib plate on the tension and compression box are taken into consideration in simulation process; in the theoretical research, the pull rod is simplified as elastic rod with uniform section, but the rib plate structure in tension and compression box is ignored; the tension and compression box is

simplified as a rigid body, these structural deviations will have an impact on transmission of stress wave in system and cause deviation between simulation results and theoretical results.

5. Conclusion

The impact mechanical system of a new hydraulic power piling machine is researched and a dynamic data modeling and simulation method of mechanical system based on meshing finite element analysis is proposed. Through LS-DYNA finite element analysis on the impact mechanical system of hydraulic power piling machine, it can be know that: (1) The LS-DYNA simulation curve and wave mechanicals theory calculation curve for impact piling force are basically similar, but the their maximum impact piling force is different. (2) From the hammer stress change cloud chart, it can be know that the stress is concentrated on the contact point of punch hammer and spring, the spring should be uniformly arranged or the crash pad can be used to replace the spring to reduce stress concentration of punch hammer.

Acknowledgement

Research project of Guangxi Education Department: Product Collaborative Design Based on 3D CAD and PDM (LX2014552).

References

[1] K. Miller, K. Chinzei, G. Orssengo, et al.: *Mechanical properties of brain tissue in-vivo: experiment and computer simulation*[J]. Journal of biomechanics, *33* (2000), No. 11, 1369–1376.

[2] C. A. Felippa, K. C. Park, C. Farhat: *Partitioned analysis of coupled mechanical systems*[J]. Computer methods in applied mechanics and engineering, *190* (2001), No. 24, 3247–3270.

[3] C. Basdogan, S. De, J. Kim J., et al.: *Haptics in minimally invasive surgical simulation and training*[J]. IEEE computer graphics and applications, *24* (2004), No. 2, 56–64.

[4] M. Friswell, J. E. Mottershead: *Finite element model updating in structural dynamics*[M]. Springer Science & Business Media (2013).

[5] F. Cirak, M. J. Scott, E. K. Antonsson, et al.: *Integrated modeling, finite-element analysis, and engineering design for thin-shell structures using subdivision*[J]. Computer-Aided Design, *34* (2002), No. 2, 137–148.

[6] O. Kolditz, S. Bauer, L. Bilke, et al.: *OpenGeoSys: an open-source initiative for numerical simulation of thermo-hydro-mechanical/chemical (THM/C) processes in porous media*[J]. Environmental Earth Sciences, *67* (2012), No. 2, 589–599.

[7] K. Mao, B. Li, J. Wu, et al.: *Stiffness influential factors-based dynamic modeling and its parameter identification method of fixed joints in machine tools*[J]. International Journal of Machine Tools and Manufacture, *50* (2010), No. 2, 156–164.

[8] C. J. Li, H. Lee: *Gear fatigue crack prognosis using embedded model, gear dynamic model and fracture mechanics*[J]. Mechanical systems and signal processing, *19* (2005), No. 4, 836–846.

[9] D. A. Steinman, J. S. Milner, C. J. Norley, et al.: *Image-based computational simulation of flow dynamics in a giant intracranial aneurysm*[J]. American Journal of Neuroradiology, *24* (2003), No. 4, 559–566.

[10] K. Miller, G. Joldes, D. Lance, et al.: *Total Lagrangian explicit dynamics finite element algorithm for computing soft tissue deformation*[J]. International Journal for Numerical Methods in Biomedical Engineering, *23* (2007), No. 2, 121–134.

[11] Y. Y. Zhang, J. W. Chan, A. Moretti, and K. E. Uhrich: *Designing Polymers with Sugar-based Advantages for Bioactive Delivery Applications*, Journal of Controlled Release, *219* (2015), 355–368.

[12] Y. Y. Zhang, Q. Li, W. J. Welsh, P. V. Moghe, and K. E. Uhrich: *Micellar and Structural Stability of Nanoscale Amphiphilic Polymers: Implications for Anti-atherosclerotic Bioactivity*, Biomaterials, *84* (2016), 230–240.

[13] J. W. Chan, Y. Y. Zhang, and K. E. Uhrich:*Amphiphilic Macromolecule Self-Assembled Monolayers Suppress Smooth Muscle Cell Proliferation*, Bioconjugate Chemistry, *26* (2015), No. 7, 1359–1369.

[14] D. S. Abdelhamid, Y. Y. Zhang, D. R. Lewis, P. V. Moghe, W. J. Welsh, and K. E. Uhrich: *Tartaric Acid-based Amphiphilic Macromolecules with Ether Linkages Exhibit Enhanced Repression of Oxidized Low Density Lipoprotein Uptake*, Biomaterials, *53* (2015), 32–39.

Received May 7, 2017